pubs.acs.org/Biomac

Article

Controllable Singlet Oxygen Generation in Water Based on Cyclodextrin Secondary Assembly for Targeted Photodynamic Therapy

Xianyin Dai, Xiaoyun Dong, Zhixue Liu, Guoxing Liu, and Yu Liu*

Cite This: *Biomacromolecules* 2020, 21, 5369−5379

Read Online

ACCESS | Metrics & More | Article Recommendations | Supporting Information

ABSTRACT: The construction of supramolecular assembly whose singlet oxygen ($^1O_2$) generation capability can be controllably regulated in water still remains challenging. Herein, a novel cyclodextrin secondary assembly was fabricated from the photochromic-switch moiety diarylethene-bridged dicyclodextrin, the adamantane-polypyridyl ruthenium photosensitizer, and the cancer-cell-targeting ligand β-cyclodextrin-grafted hyaluronic acid, which not only possessed cancer-cell-targeting ability but also served as cell imaging and photodynamic therapy agents with noninvasive controllability. In virtue of the multivalent interactions between the three components, they could self-assemble in two stages to form uniform spherical nanoparticles (OF-NPs) with average diameters of about 80 nm, as indicated by scanning electron microscopy, high-resolution transmission electron microscopy, atomic force microscopy, and dynamic light scattering. Significantly, the prepared OF-NPs exhibited excellent photochromic performance and can transform into their ring-closed form (CF-NPs), accompanied by the efficient energy transfer from donor 2 to CF-1 and gradual quenching of $^1O_2$ generation. Cellular imaging experiments showed that OF-NPs could specifically target the mitochondria of A549 cancer cells, while CF-NPs displayed a negligible red fluorescence signal in A549 cells due to the energy-transfer process. Furthermore, in vitro cytotoxicity tests revealed that upon irradiation with 450 nm light, OF-NPs with 10 μM concentration displayed a remarkable higher cytotoxicity with the cell death rate of up to 88% toward A549 cancer cells, which was approximately 4.4 times higher than that of CF-NPs. Additionally, the apoptosis rate of A549 cells induced by OF-NPs under light irradiation was 4.68 times higher than that of CF-NPs. These well-designed cyclodextrin secondary assemblies successfully achieve noninvasive control over the generation of $^1O_2$ both in water and in cancer cells by irradiation at distinct wavelengths and are further applied in targeted PDT, which avoid the inadvertent photosensitizer activation and provide a new approach for cancer therapy with more safety and high efficiency.

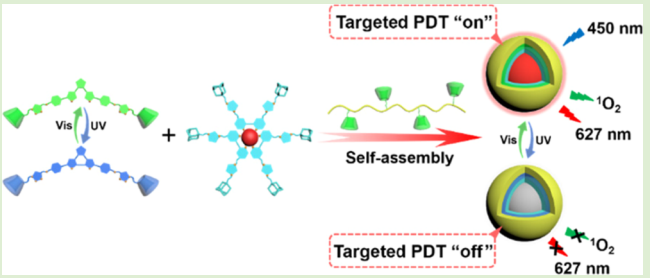

INTRODUCTION

Supramolecular assemblies with singlet oxygen ($^1O_2$) generation properties have attracted increasing attention owing to their extensive application prospects in the fields of organic catalysis,[1−5] deleterious substance degradation,[6−8] and photodynamic therapy (PDT).[9−13] Generally, $^1O_2$ is generated via the triplet−triplet energy transfer between the ground-state oxygen and the triplet-state photosensitizer derived from intersystem crossing when excited.[14,15] Recently, PDT utilizing reactive oxygen species, especially $^1O_2$, to cause irreversible damage to tumor cells has thrived as a promising approach for the treatment of various cancers.[16,17] In addition, the development of activatable photosensitizers whose $^1O_2$ generation can be modulated on demand is of great significance, which can largely avoid inadvertent photosensitizer activation to prevent unnecessary injury to the human body over the duration of treatment.[18] More specifically, the photosensitizer can be activated within the cell when responsive to various intracellular stimuli such as adenosine triphosphate, pH, and redox conditions.[19−23] However, these regulation processes are irreversible, which may lead to imprecise and uncontrollable $^1O_2$ generation. Among these stimuli, light is identified as a good option to realize the reversible photocontrol of the singlet oxygen generation because of its clean, noninvasive, and remote-controlling characteristics.[24−27]

Recently, a number of controllable $^1O_2$ generation systems based on the combination of porphyrin/dithienylethene have been successfully designed in bicomponent coordination complexes,[28] metal−organic frameworks,[29] silica-coated upconversion nanoparticles,[30] micelles,[31] and supramolecular

Received: October 27, 2020
Revised: November 17, 2020
Published: November 30, 2020

https://dx.doi.org/10.1021/acs.biomac.0c01547
Biomacromolecules 2020, 21, 5369−5379

metallacycles.[32] For example, Yang et al. designed a novel metallacycle, which combines a photochromic switch and a photosensitizer and is noncovalently encapsulated in the amphiphilic polymer mPEG-DSPE, achieving the $^1O_2$ generation on/off in vitro and in vivo.[32] Our group also previously constructed a supramolecular assembly comprising a porphyrin derivative and permethyl-β-cyclodextrin-modified dithienylethene for controlled $^1O_2$ generation in aqueous solution with 1% ethanol.[33] To date, although supramolecular systems based on diarylethene switches and porphyrin derivative to realize noninvasive control over $^1O_2$ generation have made great progress, such systems with favorable water solubility, biocompatibility, biodegradability, and cancer-cell targeting ability for application in PDT are rarely reported and still have great opportunities and challenges.

Cyclodextrins are considered as star molecules because of their low toxicity, good biocompatibility, and characteristic host−guest properties.[34−36] In particular, supramolecular nanoassemblies based on cyclodextrins have been extensively applied in biomedical areas such as dynamic biothiol sensing,[37] drug/gene delivery.[38−41] and organelle dysfunction or aggregation.[42−44] On the other hand, hyaluronic acid (HA) as a polysaccharide with water solubility, biocompatibility, and biodegradablity has been proven to be a specific tumor-cell-targeting molecule since overexpressed HA receptors were distributed on the cancer cell surface in contrast to normal cells.[42] For example, HA as a cancer-cell-targeting ligand could be integrated into a supramolecular polymer to realize ultralong room-temperature phosphorescence and targeted cancer cell mitochondria phosphorescent imaging.[45]

In this work, we constructed a novel cyclodextrin secondary assembly containing the photochromic-switch moiety diarylethene-bridged cyclodextrin (1), the adamantane-polypyridyl ruthenium photosensitizer (2), and β-cyclodextrin-grafted hyaluronic acid (HA-CD) through a host−guest recognition strategy in aqueous solution. The introduction of the β-cyclodextrin moiety into the diarylethene skeleton not only endowed 1 with decent water solubility and biocompatibility but also provided additional binding sites with 2 in virtue of the noncovalent association between cyclodextrin and adamantane. Such supramolecular aggregates 2/OF-1 could further assemble with HA-CD through host−guest interactions and electrostatic interactions, thus realizing the secondary assembly to obtain supramolecular nanoparticles (OF-NPs) with a uniform morphology and size. It was found that OF-1 still retained its excellent photochromic performance in the resultant nanoparticles, consequently contributing to the high FRET efficiency and photocontrolled $^1O_2$ generation ability in water. In addition, on account of the overexpressed HA receptors on the cancer cell surface, the formed NPs could be exclusively ingested by A549 cells and mainly distributed in the mitochondria. More importantly, the NPs could achieve the switching on/off of the singlet-oxygen generation within cells by using different wavelength light irradiation to regulate the open/closed form of diarylethene in OF-NPs/CF-NPs.

EXPERIMENTAL SECTION

Materials. All chemicals and solvents were from commercial suppliers unless otherwise stated. Alkynyl-modified diarylethene (DAE-≡) was synthesized according to the reported procedures.[33] Hyaluronic acid was purchased from Shandong Freda Biopharm Co. HA-CD was synthesized by referring to the reported procedures.[42] The recrystallization of β-cyclodextrin was performed twice in water and dried under vacuum at 90 °C for 24 h before the experiment. Analytical thin layer chromatography (TLC, GF254) was used to real-time measure the reaction process. Column chromatography with 200−300 mesh silica gel was employed for the separation and purification of target products.

Synthesis of Photochromic-Switch Moiety 1. DAE-≡ (50 mg, 0.08 mmol) and 231 mg 6-deoxy-6-azido-β-CD (0.2 mmol) were mixed in anhydrous DMF (5 mL), and 38 mg CuI (0.2 mmol) was subsequently added to the mixture. The solution was then heated to reflux in an N_2 atmosphere for 24 h. TLC was used to monitor the reaction. After cooling, any insoluble copper salt was removed from the mixture by filtration. Then, the residue was purified by MPLC (reversed phase), with water/ethanol as an eluent to give 1 as a green solid (146 mg, yield 62%). ^{1}H NMR (400 MHz, DMSO-d_6, ppm) δ 8.19 (s, 1H), 7.58 (d, J = 8.7 Hz, 1H), 7.39 (s, 1H), 7.10 (d, J = 8.4 Hz, 1H), 6.02−5.57 (m, 6H), 5.13 (s, 1H), 5.05 (s, 1H), 4.92 (d, J = 13.6 Hz, 1H), 4.81 (d, J = 21.7 Hz, 2H), 4.52 (dd, J = 32.1, 19.2 Hz, 3H), 4.33 (d, J = 17.0 Hz, 1H), 4.00 (s, 1H), 3.65 (t, J = 29.1 Hz, 9H), 3.29−3.21 (m, 1H), 3.11 (s, 1H), 2.89 (s, 1H), 1.95 (s, 1H); ^{13}C NMR (100 MHz, DMSO-d_6, ppm) δ 158.12, 158.12, 142.26, 141.71, 140.11, 126.70, 125.44, 124.94, 121.06, 115.34, 101.98, 101.22, 83.46, 82.06, 81.46, 80.94, 72.93, 72.31, 72.02, 71.72, 69.99, 61.50, 61.08, 58.98, 14.02; HRMS (ESI): m/z calcd for $C_{117}H_{160}F_6N_6O_{70}S_2Na^+$, 2971.639 $[M + Na^+]^+$; found: 2971.646.

Synthesis of Adamantane-Polypyridyl Ruthenium Photosensitizer 2. Bipyridine imidazolium e (188 mg, 0.23 mmol, 3.1 eq) and 37 mg of $Ru(dmso)_4Cl_2$ (0.075 mmol, 1.0 eq) were mixed in EtOH (10 mL). The reaction mixture was kept at reflux overnight in the dark under an N_2 atmosphere. Rotary evaporation was used to remove the solvents, and the obtained crude red residue was redissolved in a small amount of water; 100 mg of ammonium hexafluorophosphate was added and orange precipitate was obtained; it was filtered to obtain an orange solid. Then, the solid was dissolved into 10 mL of CH_3CN, and 90 mg of tetrabutylammonium chloride was added, and red precipitate was obtained, which was filtered to obtain an orange solid, and the product was washed with CH_3CN three times, separately. A dark red power was obtained after vacuum drying (yield: 50%). ^{1}H NMR (400 MHz, DMSO-d_6, ppm) δ 9.65 (s, 2H), 9.28 (s, 2H), 8.09 (s, 2H), 7.80 (d, J = 5.9 Hz, 2H), 7.69 (s, 2H), 7.49 (d, J = 5.8 Hz, 2H), 5.81 (s, 4H), 5.72 (s, 4H), 2.04 (s, 6H), 1.87 (s, 12H), 1.71 (dd, J = 29.0, 12.0 Hz, 12H); ^{13}C NMR (100 MHz, DMSO-d_6, ppm) δ 206.94, 157.01, 152.53, 146.15, 138.85, 127.60, 124.81, 122.82, 54.73, 50.49, 45.27, 37.62, 36.31, 27.64; HRMS (ESI): m/z calcd for $C_{126}H_{146}N_{18}O_6Ru^{4+}$ 527.2671 $[M - 8Cl^- - 4H^+]^{4+}$, found: 527.2694; m/z calcd for $C_{126}H_{145}N_{18}O_6Ru^{3+}$ 702.6879 $[M - 8Cl^- - 5H^+]^{3+}$, found: 702.6891.

Synthesis of β-Cyclodextrin-Grafted Hyaluronic Acid HA-CD. Sodium hyaluronate (250 mg, M_w = 200,000, 1.25 μmol) was added into 150 mL of 0.1 M PBS (pH 7.2), and the mixture was stirred vigorously for 30 min at 25 °C until completely dissolved. Then, 419 mg of 1-ethyl-3-(3-dimethyl aminopropyl)-carbodiimide hydrochloride (2.2 mmol) and 253 mg of *N*-hydroxysuccinimide (2.2 mmol) were added successively. Then, 2942 mg of mono-6-deoxy-6-ethylenediamino-β-CD (2.5 mmol) in 50 mL of PBS was added to the above solution, and the mixture was stirred for 24 h at 25 °C. Finally, the resulting solution was dialyzed with excess pure water for 7 days, and the water was changed every 12 h. After freeze-drying, the desired product HA-CD was obtained as a white fluffy powder. The grafted β-CD on the conjugate was measured by the ^{1}H NMR integral of the corresponding characteristic peak. ^{1}H NMR (400 MHz, D_2O, ppm) δ 5.05 (s, 2.35H), 4.48 (d, J = 27.2 Hz, 2.03H), 4.09−3.14 (m, 5.54H), 1.98 (s, 2.8H).

Preparation of Nanoparticles (NPs). The stock solutions of NPs were prepared by dissolving 2.40 mg of compound 2 (1.0 mmol) and 8.85 mg of OF-1 (3.0 mmol) in 1 mL of deionized water. Next, 2.32 mg HA-CD involving around 1.0 mmol β-CD was mixed with the above solution. Finally, the mixed solution was homogenized by ultrasound for 10 min and kept in a refrigerator at 4 °C for further use.

https://dx.doi.org/10.1021/acs.biomac.0c01547
Biomacromolecules 2020, 21, 5369−5379

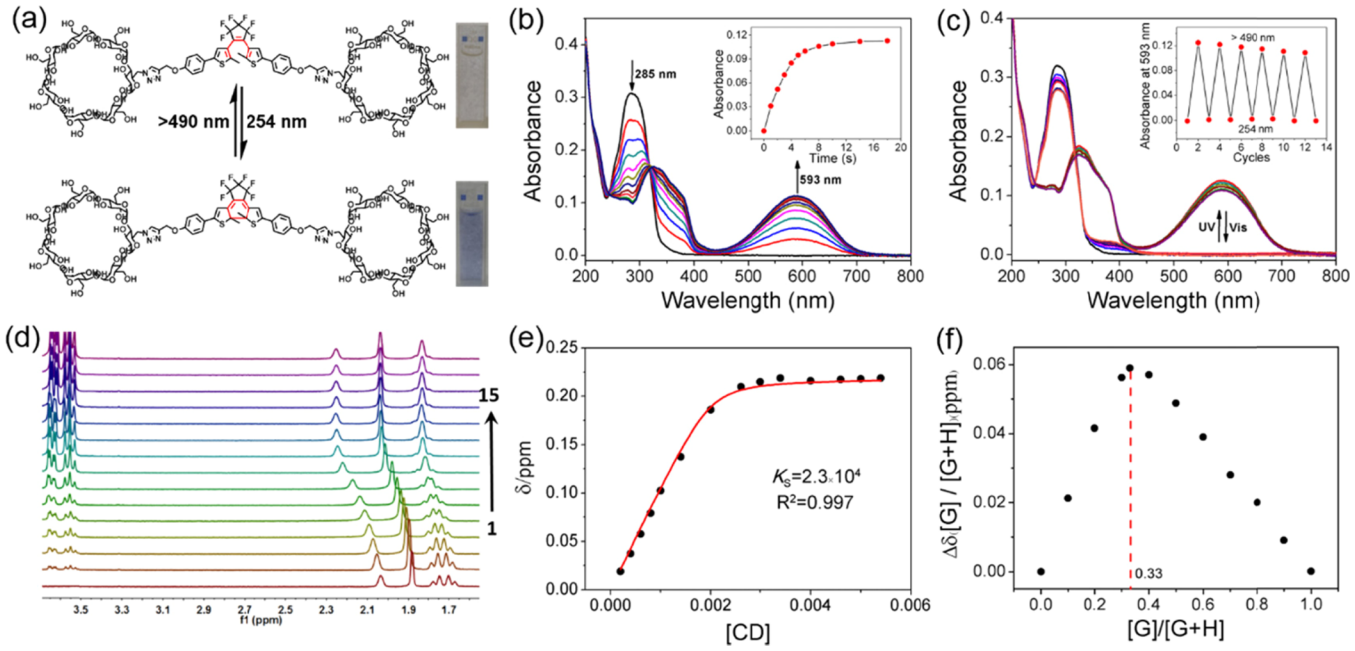

Figure 1. (a) Constitutional formula and color changes of 1 under alternant UV and visible light irradiation. (b) UV−vis spectra changes of OF-1 (10 μM) under UV light (254 nm) irradiation in aqueous solution. Inset: Absorbance intensity changes of 1 at 593 nm. (c) UV−vis spectra of 1 under alternant UV light and visible-light (>490 nm) irradiation. Inset: Absorbance intensity changes at 593 nm after multiple irradiation cycles. ^{1}H NMR titration of e by using native β-CD. (d) ^{1}H NMR spectra of e (1 mM) with 0, 0.2, 0.4, 0.6, 0.8, 1.0, 1.4, 2.0, 2.6, 3.0, 3.4, 4.0, 4.6, 5.0, and 5.4 mM β-CD (from 1 to 15) in D_2O at 25 °C. (e) Chemical shift changes of e peaks at d = 2.03 ppm vs the concentration of β-CD by using the nonlinear least-squares fitting method. (f) Job plot toward the binding of e (G) with β-CD (H) in D_2O ([e] + [β-CD] = 1 mM) at 25 °C.

Cellular Uptake Study. A549 cells and 293T cells were subcultured into a confocal Petri dish and cultured for 24 h at 37 °C in a humidified 5% CO_2 atmosphere, separately. A549 cells were divided into two groups and then incubated with OF-NPs (5 μM) and CF-NPs (5 μM), and 293T cells were treated with OF-NPs under the same conditions. After 24 h coincubation, the culture medium was discarded, and the cells were washed with 0.01 M PBS at least three times. The fluorescence images were acquired by CLSM.

Colocalization Imaging. A549 cells were first subcultured into a confocal petri dish and incubated for 24 h at 37 °C in a humidified 5% CO_2 atmosphere, and then, OF-NPs were added into the dish to ensure that their concentration is 5 μM in the culture medium and cultured for another 24 h. After this, the culture medium was discarded, and the cells were washed with 0.01 M PBS at least three times. Next, MitoTracker Green cocultured with the cells at 37 °C for 30 min to stain the mitochondria. After the cells were repeatedly washed at least three times with PBS, the localization of the nanoparticles in the cells was immediately observed by CLSM. The excitation wavelength was set as 488 nm, and the emission was collected from 510−540 nm for MitoTracker Green. The excitation wavelength was set as 458 nm and the emission was collected from 600−650 nm for OF-NPs.

Extracellular $^1O_2$ Detection. Commercial ABDA was exploited as a tracer agent to access the differences in the $^1O_2$ production efficiencies of different samples. In particular, each sample and ABDA were together dispersed in 3 mL of deionized water with a final concentration at 0.01 mM and 0.05 mM, respectively. Then, the mixed solution was irradiated with 450 nm light with a power of 220 mW/cm^2. The $^1O_2$ generation efficiency was measured by monitoring the UV−vis absorbance change of ABDA at 378 nm in different irradiation time intervals.

$^1O_2$ Generation Quantum Yields. $[Ru(bpy)_3]Cl_2$ (Φ_Δ = 0.18 in H_2O) was utilized as a standard, and ABDA was used as an indicator to assess the quantum yields for the $^1O_2$ generation of different samples under irradiation.[46] Typically, deionized water solutions with different samples and ABDA (50 μM) were mixed well under dark conditions and then exposed to 450 nm light. The absorbance of ABDA at 378 nm were recorded every 20 s. The Φ_Δ of the samples was calculated according to the following formula:

$$\Phi_{\Delta(x)} = \Phi_{\Delta(\mathrm{std})} \times \frac{S_x}{S_{\mathrm{std}}} \times \frac{F_{\mathrm{std}}}{F_x}$$

where subscripts std and x, respectively, represent the $[Ru(bpy)_3]Cl_2$ and sample; S indicates the slope of the absorbance of ABDA at 378 nm versus irradiation time (s); and F, which is obtained by $F = 1-10^{-\mathrm{OD}}$, represents the absorbance correction factor (OD signifies the optical density of $[Ru(bpy)_3]Cl_2$ and the sample at 450 nm).

Intracellular $^1O_2$ Detection. The intracellular $^1O_2$ generation of nanoparticles was studied via a common ROS indictor, 2′,7′-dichlorofluorescin diacetate (DCFH-DA). First, the A549 cancer cells were coincubated with 10 μM each sample for 24 h. After 24 h incubation, DCFH-DA was added into the culture medium with incubation for 15 min. Then, the cells were washed with 0.01 M PBS at least three times to remove excess DCFH-DA, and the new culture medium was added, followed by irradiation with 450 nm light irradiation for 5 min. Finally, the intracellular $^1O_2$ level was examined immediately by CLSM. The excitation was set as 488 nm, and the emission wavelength was collected from 500 to 530 nm.

In Vitro Cytotoxicity Tests. First, A549 cells or 293T cells were plated into 96-well plates and incubated for 24 h. After this, the cells were treated with OF-NPs or CF-NPs at a serial of concentrations from 0 to 10 μM for another 24 h in the absence of light. Subsequently, the cells were exposed to 450 nm light irradiation for 30 min. Then, the cells were allowed to continue growing for another 1 h. The culture medium was discarded, and the cells were washed with 0.01 M PBS twice. Then, CCK8 solution was added to each well, and the cells were further incubated at 37 °C for 1 h. The absorbance value was obtained using a microplate reader at 450 nm wavelength. The data were all displayed as the mean ± standard deviation. The NP concentrations were on the basis of photosensitizers.

Cell Apoptosis Assay. A549 cells were plated into six-well plates and divided into three groups: control, treatment with CF-NPs, and treatment with OF-NPs. Then, the cells were incubated in the dark at 37 °C for 24 h. The cells were irradiated with 450 nm light for 30 min.

https://dx.doi.org/10.1021/acs.biomac.0c01547
Biomacromolecules 2020, 21, 5369−5379

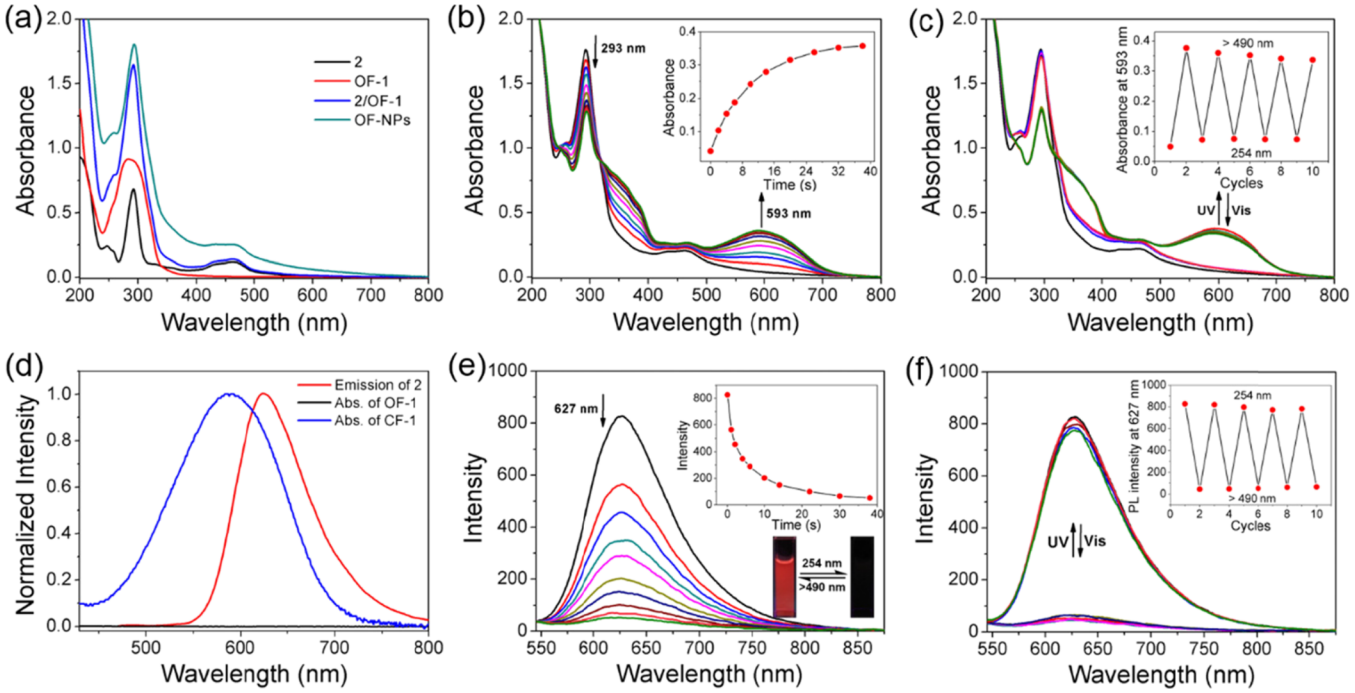

Figure 2. (a) Absorption spectra of 2, OF-1, 2/OF-1, and OF-NPs. (b) UV−vis spectra changes of OF-NPs ([2] = 10 μM, [OF-1] = 30 μM, [HA-CD] = 10 μM) under UV light irradiation in aqueous solution. Inset: Absorbance intensity changes of OF-NPs at 593 nm. (c) UV−vis spectra of OF-NPs under alternant UV light and visible-light irradiation. Inset: Absorbance intensity changes at 593 nm upon repeated alternating UV/vis irradiation. (d) Normalized absorption spectra of OF-1 and CF-1 and emission spectra of 2. (e) Emission spectra of OF-NPs upon irradiation with UV light (λ_{ex} = 450 nm) in aqueous solution. Inset: Emission intensity changes at 627 nm. (f) Emission spectra changes at 627 nm for OF-NPs in aqueous solution under alternant UV light and visible-light irradiation. Inset: Fluorescent reversibility for OF-NPs detected by the emission intensity change at 627 nm with five cycles.

Finally, the cells were digested by using trypsin and resuspended in 100 μL of binding buffer, and annexin VFITC/PI was used to stain the cells for 10 min away from light before detection by flow cytometry.

RESULTS AND DISCUSSION

The brief synthesis routes of symmetrical host OF-1 and guest 2 are shown in Schemes S1−S4 and fully characterized by ^{1}H NMR, ^{13}C NMR, and HR-MS (Figures S1−S12). The diarylethene-bridged dicyclodextrin 1 was prepared in 62% yield via the click reaction between alkynyl-modified diarylethene and 6-deoxy-6-azido-β-CD by using CuI as the catalyst in anhydrous DMF. Guest 2 was obtained in 50% yield through the complexation between adamantane-modified 2,2′-bipyridine imidazolium e and $Ru(dmso)_4Cl_2$ in anhydrous ethanol. Subsequently, the reversible photochromic performance of 1 was investigated detailedly in aqueous solution. As shown in Figure 1b, host 1 gave a strong maximum absorption at 285 nm when it was in the open form (OF-1). When irradiated with UV light (254 nm) for 18 s, OF-1 gradually underwent the photoisomerization process with the appearance of a new peak centered at 593 nm and the simultaneous decrease of the peak centered at 285 nm in UV−vis spectra. Meanwhile, an isoabsorption point appeared at 320 nm, which further proved that the OF-1 transformed into the closed form (CF-1). This process could also be observed with the naked eye that the aqueous solution of OF-1 changed from colorless to blue after UV illumination (Figure 1a, inset). The blue color of CF-1 not only reverted to its original colorless state, but also its UV absorption generally restored to the initial level upon irradiation with visible light (>490 nm), suggesting the reversible conversion from CF-1 to OF-1. Importantly, such a reversible photochromic switch displayed favorable reversibility and excellent fatigue resistance under alternant UV and visible light irradiation at least six times (Figure 1c). ^{1}H NMR was also used to monitor this reversible photocyclization/reversion process. As shown in Figure S14, the protons on the diarylethene skeleton of OF-1 showed different degrees of chemical shifts with the prolongation of the UV irradiation time until they reached the photostable state, and the ring-closing conversion rate for the transformation from OF-1 to CF-1 was approximately determined as 95% by the ^{1}H NMR integral of the final product after UV illumination. More interestingly, a complete recovery of the ^{1}H NMR spectra OF-1 was observed when CF-1 was irradiated with visible light (>490 nm), indicating that CF-1 could be quantitatively converted back to OF-1 (Figure S15).

Benefiting from the introduction of β-cyclodextrin (β-CD) units, OF-1 was allowed to hold remarkable water solubility, and the binary supramolecular assemblies could be facilely fabricated by directly mixing OF-1 and 2 due to the extraordinary recognition capability between the β-CD cavity and the adamantane moiety in aqueous solution. A synthetic intermediate adamantane-modified 2,2′-bipyridine imidazolium e was employed as a reference guest and native β-CD was used as a reference host for ^{1}H NMR titration to investigate the supramolecular interactions between OF-1 and 2. As displayed in Figure 1d, the proton signals of adamantane shifted downfield from d = 2.03 ppm to d = 2.25 ppm gradually along with the shape changes when the concentration of β-CD was increased from 0 to 5.4 mM. This observation suggested that the adamantane was included into the β-CD cavity. Other

https://dx.doi.org/10.1021/acs.biomac.0c01547
Biomacromolecules 2020, 21, 5369−5379

than that, the binding constant (K_S) was calculated as 2.3×10^4 M^{-1} through analyzing the titration data via the nonlinear least-squares fitting method (Figure 1e). In addition, Job analysis showed a maximum value at a molar fraction of 0.33, confirming that the binding stoichiometry between e and β-CD was 1:2. In addition, the 2D ROESY spectra (Figure S16) in D_2O clearly showed the visible ROE signals between the adamantanyl protons and β-CD, which demonstrated that that the adamantanyl part of e was located in the β-CD cavity.

The UV−vis absorption spectra of 2 presented two typical peaks of $[Ru(bpy)_3]^{2+}$, corresponding to the ligand−ligand charge transfer and metal−ligand charge transfer at 292 and 463 nm (Figure 2a), respectively. Upon being excited at 450 nm, 2 emitted bright orange-red fluorescence whose maximum emission was at 627 nm (Figure S17). It is well known that a good spectral overlap between the emission of the donor and the absorption of the acceptor was beneficial to promote the occurrence of the efficient FRET process. As mentioned, OF-1 had an intense absorption peak centered at 285 nm and showed no absorption over 400 nm, which mismatched the spectra with 2 whose fluorescence emission band is in the range of 550−850 nm; hence, the FRET process was forbidden from OF-1 to 2. However, the absorption spectra of CF-1 showed broad absorption ranging from 450 to 750 nm and had a good spectral overlap with the fluorescence emission band of 2 (Figure 2d). Therefore, we reasonably speculated that the FRET process might occur from 2 to CF-1. We first studied the FRET behavior of the binary assemblies 2/OF-1 in water. As shown in Figure S17, the 2/OF-1 gave an emission peak at 627 nm when excited at 450 nm. Compared with 2 alone, the fluorescence intensity of the resultant OF-NPs was reduced by 3.8%, which probably resulted from the photoinduced electron transfer between the diarylethene group in OF-1 and 2 after their association (Figure S17). Upon exposing the 2/OF-1 solution to UV light for 50 s, the fluorescence intensity of the 2/OF-1 was gradually quenched (Figure S18a), and the energy transfer efficiency (E) was determined to be 94.8%. Through comparison of the maximum fluorescence intensity values before and after UV light irradiation, the fluorescence on/off quenching ratio ($R_{on/off}$) was determined to be 19.3 (Figure S18b). Moreover, the quenched fluorescence could be recovered when subsequently irradiated with visible light because of the reverse photoisomerization from CF-2 to OF-2 (Figure S18c). Importantly, no apparent fatigue could be found after repeated five cycles (Figure S18d).

In the control experiment, when using diarylethylene without β-cyclodextrin modification as the acceptor, even if UV irradiation reached 242 s, the fluorescence intensity of 2 only dropped by 23.8% and the $R_{on/off}$ was calculated as 1.3 (Figure S19). A similar phenomenon was also observed when the commercially available tris(2,2′-bipyridine) ruthenium dichloride ($[Ru(bpy)_3]Cl_2$) was selected as the donor, and its fluorescence intensity was reduced by 33.6% after UV irradiation for 146 s and the calculated $R_{on/off}$ was 1.5 (Figure S20). These findings consistently illustrated that the host−guest interaction existed in adamantine, and β-cyclodextrin was extremely beneficial for the efficient energy transfer process. Besides the good spectral overlap, the center-to-center distance between the donor and the acceptor was also critical. The lack of the corresponding host−guest interactions in the two control experiments resulted in the poor energy transfer and fluorescence quenching. However, when 1 and 2 self-assembled into supramolecular assemblies in aqueous solution, the distance between them was shortened within the Förster radius, thus promoting the FRET process.

Next, the FRET process in the formed cyclodextrin secondary assemblies OF-NPs was also investigated. To our delight, the OF-NPs still showed the excellent photochromic performance and reversibility. As shown in Figure 2b, a new absorption peak centered at 593 nm emerged after UV light irradiation for 38 s and the absorption peak at 285 nm decreased simultaneously with the change in the OF-NP solution color from light yellow to blue (Figure S21), indicating that the photoisomerization process of OF-1 was not disturbed after incorporation into these nanoparticles. When irradiated with visible light (>490 nm) for 60 s, the UV absorption of CF-NPs generally restored to the initial level and the solution color of CF-NPs turned light yellow again, suggesting the reversible conversion from CF-NPs to OF-NPs (Figure S22). Significantly, these supramolecular nanoparticles exhibited good reversibility at least five times upon alternant UV and visible light irradiation without apparent fatigue (Figure 2c). Upon being irradiated with the UV light for 38 s, the fluorescence intensity of OF-NPs was gradually quenched (Figure 2e) and E was determined to be 93.7% with the fluorescence quenching ratio as 15.7. In addition, when the nonfluorescent solution of CF-NPs was exposed to visible light for 1 min, the quenched fluorescence could be restored to the previous fluorescence intensity because of the reversible photoisomerization from CF-1 to OF-1. The fluorescence quenching induced by the process could also be easily perceived with the naked eye, in which the dazzling orange-red fluorescence of OF-NPs gradually weakened to darkness under UV irradiation (Figure 2e, inset). Moreover, when exposed to visible light, the aqueous solution returned to its original orange-red fluorescence, insinuating that CF-NPs reconverted into OF-NPs. Crucially, such a photochromic switching process was able to repeat for several times without significant fatigue (Figure 2f). These phenomena jointly indicated the occurrence of the FRET process from 2 (donor) to CF-1 (acceptor) in these formed supramolecular nanoparticles. In particular, the open-ring form OF-1 within the nanoparticles underwent photoisomerization and transformed into the close-ring form CF-1 upon UV irradiation, resulting in the continuous fluorescence quenching of 2 by the gradually generated CF-1 originating from the good spectral overlap between the emission of 2 and the absorption of CF-1.

The structure information of supramolecular nanoparticles assembled from OF-1, 2, and HA-CD in two stages was fully characterized by HR-TEM, AFM, SEM, DLS, and zeta potential experiments. First, the morphology of 1 before and after UV irradiation was investigated. As depicted in Figure S23, OF-1 itself presented a scattered structure without a uniform morphology. Even after UV irradiation, the morphology of CF-1 showed negligible difference in comparison with OF-1. Then, the supramolecular nanoparticles mediated in two stages were carefully prepared and fully characterized. In the first stage, 2 could initiate the aggregation of OF-1 to form a number of tightly irregular nanoparticles with a diameter of about 36 nm on account of strong host−guest interactions, as revealed by the TEM images. Furthermore, these nanoparticles still maintained their original morphology with a slightly increased diameter of about 45 nm when converted into 2/CF-1 after UV irradiation (Figure S24). Such binary supramolecular complexes could further interact with HA-CD to form the final supramolecular nanoparticles as the second

https://dx.doi.org/10.1021/acs.biomac.0c01547
Biomacromolecules 2020, 21, 5369−5379

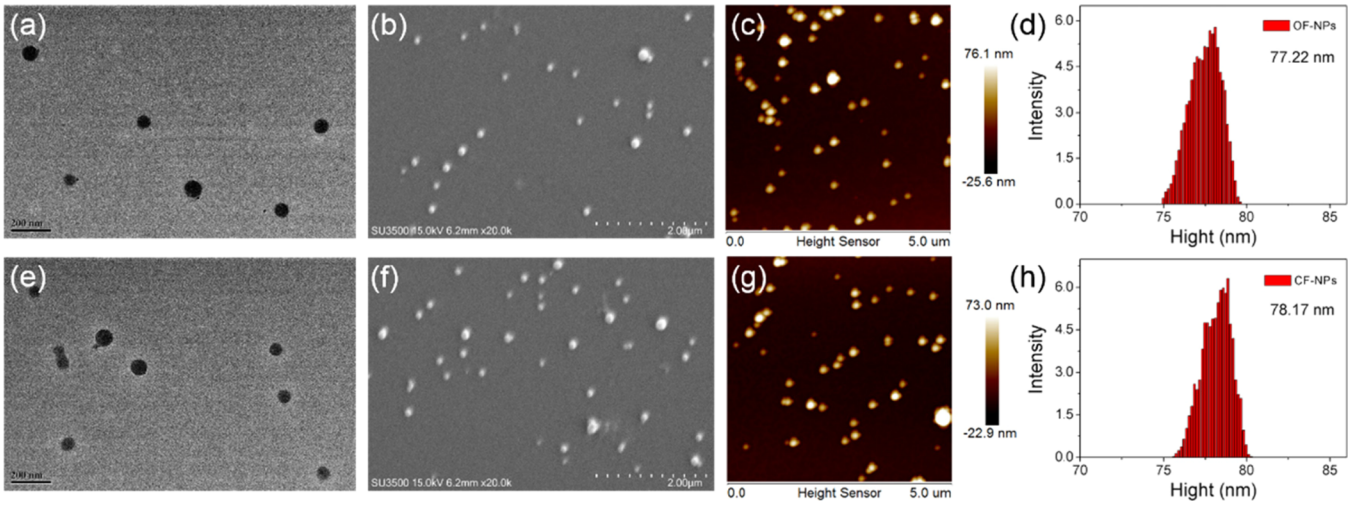

Figure 3. Characterization of the obtained cyclodextrin secondary assembly NPs. Typical (a) HR-TEM image, (b) SEM image, (c) AFM image, and (d) height histogram of OF-NPs from (c). (e) HR-TEM image, (f) SEM image, (g) AFM image, and (h) height histogram of CF-NPs from (g).

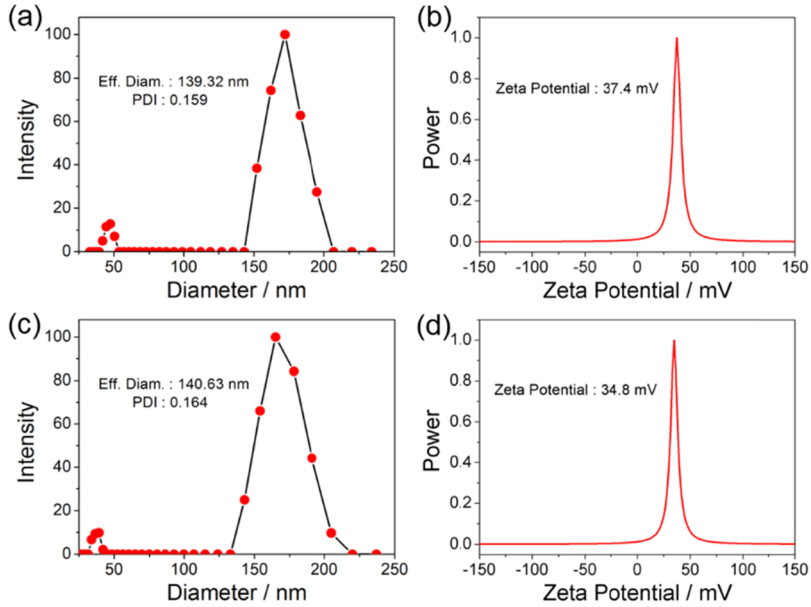

Figure 4. (a) DLS result and (b) zeta potential of OF-NPs. (c) DLS result and (d) zeta potential of CF-NPs.

stage. OF-NPs were observed as a series of uniform spherical nanoparticles with average diameters of ca. 80 nm in HR-TEM images (Figure 3a and Figure S25), which were more uniform and much larger spheres than these binary supramolecular assemblies. The SEM image (Figure 3b) also provided consistent morphological information, which showed a number of homogeneous spherical nanoparticles with a uniform size. Such evolution of self-assembled morphologies distinguished from the binary supramolecular assemblies was primarily derived from the extra multivalent interactions with HA-CD including host−guest and electrostatic interactions. Moreover, the fine structure and dimension of OF-NPs was also verified by AFM images. Numerous spherical nanoparticles were observed, and the height of these nanoparticles was determined to be 77.22 nm (Figure 3c,d), which were fairly consistent with the results of HR-TEM and SEM. Moreover, dynamic light scattering (DLS) experiments were performed for further illustration. The average hydrodynamic diameter of OF-NPs was measured as 139.32 nm with a narrow distribution, confirming the good dispersion of nanoparticles in water (Figure 4a). Notably, the diameter of OF-NPs was larger than that found in TEM, SEM, and AFM images, which probably resulted from the shrinking of nanoparticles when preparing these samples by the air-drying method. Furthermore, OF-NPs had a zeta potential as 37.4 mV (Figure 4b), presenting a significant decline compared with the binary assemblies 2/OF-1 (Figure S26), indicative of the formation of ternary supramolecular nanoparticles after coassembly with HA-CD. Meanwhile, an enhanced Tyndall effect was observed in contrast to 2/OF-1 and free OF-1 (Figure S27), further suggesting the formation of larger nanoparticles in solution. The schematic illustration for the possible formation mode of supramolecular nanoparticles is presented in Scheme 1. In addition, when OF-NPs were transformed into CF-NPs after irradiation with UV light, there was no significant difference in the HR-TEM, SEM, AFM, DLS, and zeta potential (Figure 3e-

https://dx.doi.org/10.1021/acs.biomac.0c01547
Biomacromolecules 2020, 21, 5369−5379

Scheme 1. (a) Schematic Diagram of the Formation of Cyclodextrin Secondary Assemblies (Designated as NPs) with Controllable $^1O_2$ Generation Ability and (b) Their Application for Targeted PDT and (c) Chemical Structures of Diarylethene Bridged Cyclodextrin 1 in Its Ring-Opened form (OF-1) and Ring-Closed form (CF-1), Adamantane Polypyridyl Ruthenium Photosensitizer (2) and β-Cyclodextrin-Grafted Hyaluronic Acid (HA-CD)

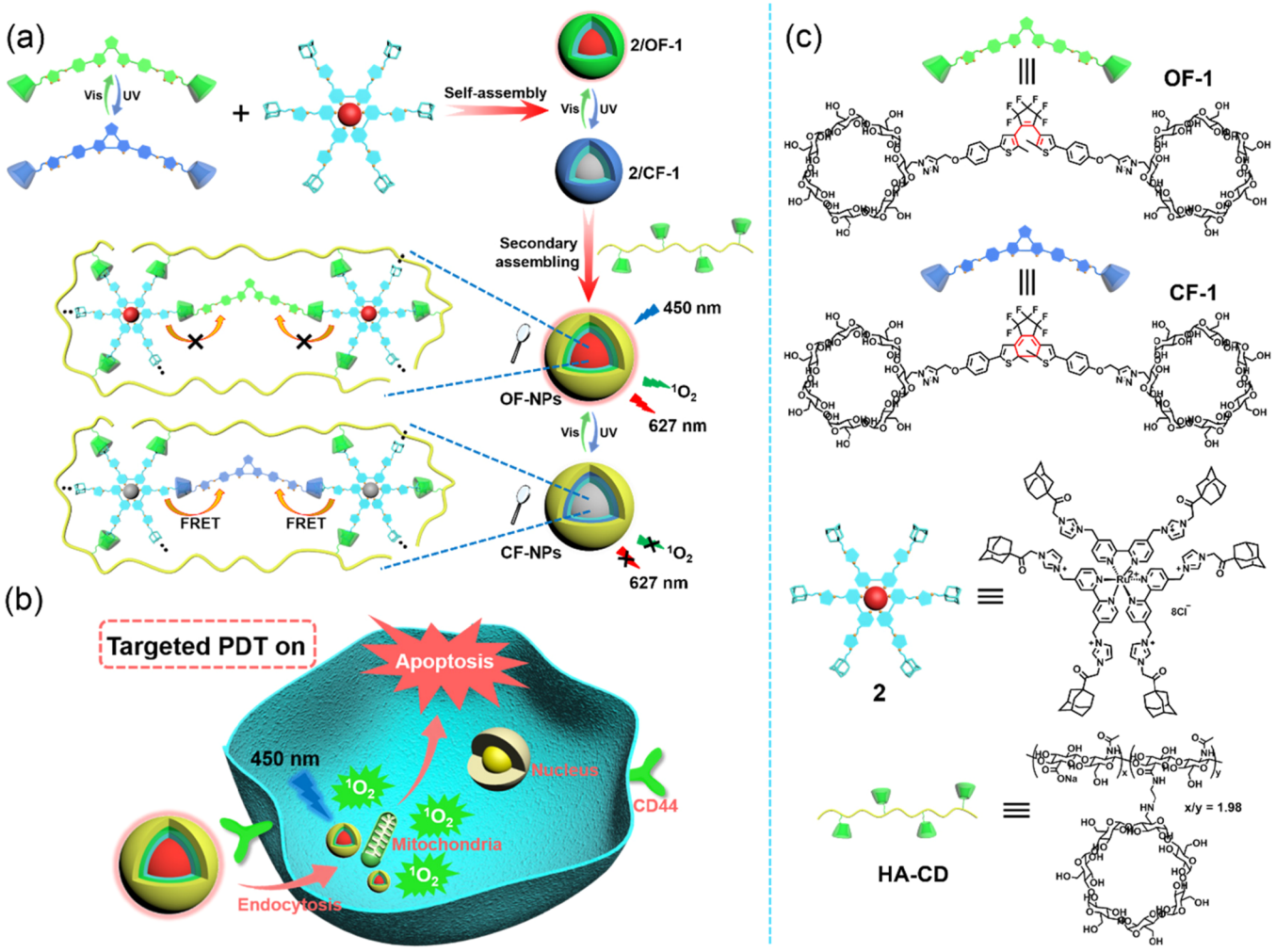

h, Figure 4c,d), illustrating the similar morphological structure in water between CF-NPs and OF-NPs. These well-defined supramolecular nanoparticles with a suitable size and a uniform morphology not only provided conditions for the occurrence of the efficient FRET process but also could be easily taken up by the cells, thus making them great candidates for subsequent cellular applications.

To evaluate the ability of these supramolecular nanoparticles for photocontrolled cell imaging, confocal laser scanning microscopy (CLSM) was performed to visualize the differences in imaging. First, a commercial mitochondrial dye, MitoTracker Green, was utilized to clarify the subcellular localization of these supramolecular nanoparticles. The A549 cells were first cocultured with OF-NPs and then stained with MitoTracker Green for 5 min. As seen in Figure 5a, the red fluorescence inside the cells was attributed to the OF-NP emission from 600 nm to 650 nm when excited by 458 nm laser, which showed a high Pearson's correlation coefficient of 0.78 with the green fluorescence from Mitotracker (Figure S28), implying the selective accumulation of OF-NPs in the mitochondria. However, 293T normal cells hardly exhibited any red fluorescence (Figure S29), indicating the poor cellular uptake of OF-NPs under the same experimental conditions.

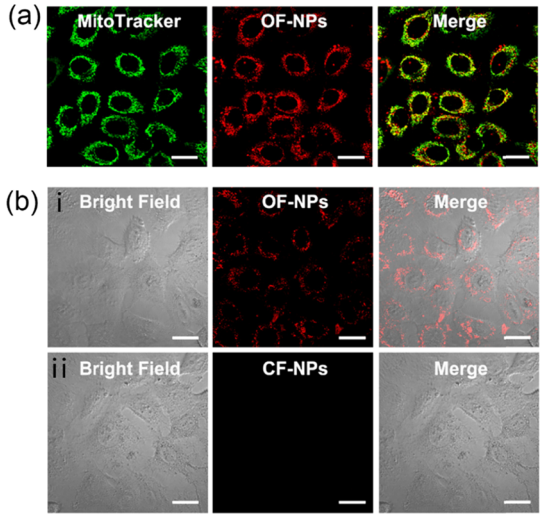

Figure 5. (a) Mitochondria colocalization images of OF-NPs in living A549 cancer cells. (b) CLSM images of A549 cancer cells treated with OF-NPs (i) and CF-NPs (ii), respectively. The scale bar is 20 μm.

https://dx.doi.org/10.1021/acs.biomac.0c01547
Biomacromolecules 2020, 21, 5369−5379

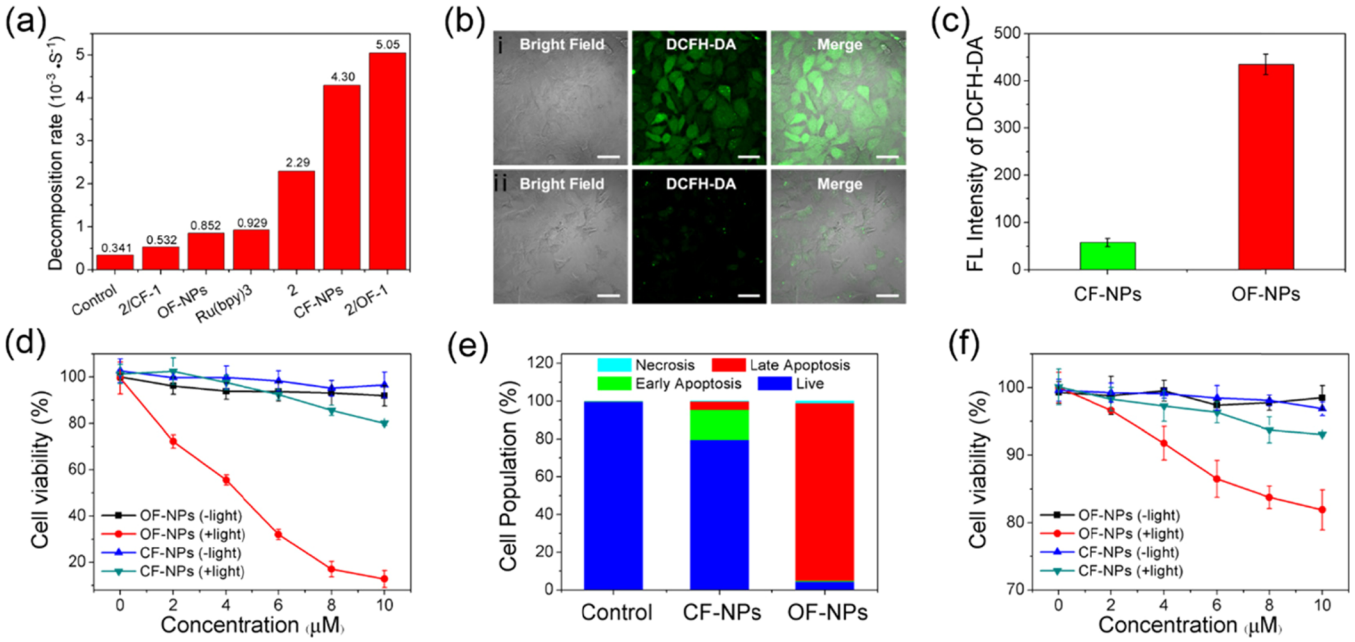

Figure 6. (a) Decomposition rate of ABDA at 378 nm in water by mixing different samples, respectively, under 450 nm light irradiation for 160 s. (b) Intracellular $^1O_2$ detection using the DCFH-DA enzyme as an indicator in A549 cancer cells after incubation with OF-NPs (i) or CF-NPs (ii) followed by 450 nm light irradiation for 5 min. The scale bar is 20 μm. (c) Quantitative fluorescence values of DCFH-DA in A549 cancer cells from (b). (d) Cell viability of A549 cancer cells after 24 h incubation with OF-NPs or CF-NPs followed by treatment with 450 nm light irradiation for 30 min or not at different concentrations. (e) Apoptosis assay of A549 cancer cells by using the Annexin V-FITC/PI dual staining method after treatment with OF-NPs or CF-NPs under 450 nm light irradiation for 30 min ([NPs] = 10 μM). (f) Cell viability of 293T normal cells after 24 h incubation with OF-NPs or CF-NPs followed by treatment with 450 nm light irradiation for 30 min or not at different concentrations.

These experimental investigations showed that the as-prepared supramolecular nanoparticles preferentially targeted cancer cells over normal cells benefiting from the over-expressed CD44 receptor on cancer cells and accumulated in the mitochondria of cancer cells with high specificity. The mitochondria-targeting ability of the nanoparticles was due mainly to the relatively positive characteristic on their surface, which contributed to their accumulation in the mitochondria with an intrinsic high negative membrane potential.[47] On the other hand, as depicted in Figure 5b, bright red fluorescence could be clearly observed when A549 cells were co-cultured with OF-NPs for 24 h, whereas almost no fluorescence signal was displayed after incubation with the ring-closed form CF-NPs under the same experimental conditions. These intracellular imaging results were consistent with the extracellular experiments, proving that the energy transfer from 2 to CF-1 in CF-NPs did occur under the excitation of the 458 nm laser, which resulted in the red fluorescence quenching of 2.

The excellent photoswitchable performance of these supramolecular nanoparticles motivated us to explore their controllability of $^1O_2$ generation in water. Commercial 9,10-anthracenediyl-bis-(methylene)-dimalonic acid (ABDA) was utilized as an $^1O_2$ capture agent to evaluate the $^1O_2$ generation ability of supermolecular nanoparticles in aqueous solution under xenon lamp irradiation with a 450 nm filter. We adopted 450 nm as the excitation wavelength for $^1O_2$ generation to avoid the potential interference for the photoswitch. ABDA would show a significant decrease in absorption when capturing $^1O_2$ due to the destruction of the probe core structure. ABDA was mixed with the corresponding solution and then irradiated with 450 nm light; subsequently, the changes in the absorption of ABDA were recorded according to the time. As shown in Figure S30, no apparent deterioration could be observed when free ABDA was treated with 450 nm light illumination for 160 s. In addition, ABDA displayed negligible decomposition under the same treatment as above, suggesting that neither OF-1 nor CF-1 were able to generate any obvious $^1O_2$ (Figure S31). However, 2 gave rise to the remarkable decomposition of ABDA under the same experimental conditions (Figure S32b). Importantly, after assembling with OF-1 into supramolecular nanoparticles, 2/OF-1 induced a significantly faster decline in ABDA absorption, explaining 2/OF-1 held a better $^1O_2$ generation efficiency than free 2. However, when 2/OF-1 was converted into 2/CF-1 after irradiation with UV light, 2/CF-1 almost completely inhibited the $^1O_2$ production under the same conditions. Similar experimental phenomena could also be found in the OF-NP and CF-NP groups (Figure S32). Moreover, $[Ru(bpy)_3]Cl_2$ was chosen as a reference to assess the $^1O_2$ production quantum yields of these samples under irradiation. As illustrated in Figure 6a, the decomposition rate constants of $[Ru(bpy)_3]Cl_2$ and 2 were determined as 0.929×10^{-3} S^{-1} and 2.29×10^{-3} S^{-1} by fitting the curve of ln (A_0/A) versus irradiation time (Figure S33), whereas those of 2/OF-1 and 2/CF-1 were 5.05×10^{-3} S^{-1} and 0.532×10^{-3} S^{-1}, respectively. By comparison with $[Ru(bpy)_3]Cl_2$ whose $^1O_2$ quantum yield was 0.18 in H_2O,[46] this value of 2 was obtained as 0.42. It was worth mentioning that 2/OF-1 presented an $^1O_2$ quantum yield as high as 0.93 among these samples, which was about 7.2 times larger than that of 2/CF-1 whose $^1O_2$ quantum yield was measured as 0.13 under the same experimental conditions. Additionally, after secondary assembly with HA-CD to form OF-NPs, they also caused a notable decomposition of ABDA under the same experimental conditions, indicating their high $^1O_2$ generation efficiency. The $^1O_2$ generation quantum yield decreased slightly from

https://dx.doi.org/10.1021/acs.biomac.0c01547
Biomacromolecules 2020, 21, 5369−5379

0.93 to 0.61 compared with 2/OF-1, while this value was around 8.7 times higher than that of CF-NPs whose $^1O_2$ quantum yield was determined as 0.07 after the transformation via 254 nm UV irradiation, verifying the photocontrolled singlet oxygen generation ability of these supramolecular nanoparticles in water.

We further investigated the differences in intracellular ROS levels caused by OF-NPs or CF-NPs via a commercially available ROS indicator DCFH-DA whose green fluorescence could be turned on in the presence of ROS in living cells. As shown in Figure 6b, A549 cells treated with OF-NPs exhibited obviously strong green fluorescence in 500−530 nm, while the A549 cells treated with CF-NPs according to the same procedure showed an inappreciable green fluorescence signal. The strong green fluorescence originated from the reaction between the indicator and the singlet oxygen produced by OF-NPs. The quantitative analysis of the fluorescent intensity in Figure 6b is shown in Figure 6c. The intracellular fluorescence intensity arising from OF-NPs under 450 nm light irradiation was approximately 7.5 times stronger than that of CF-NPs, implying that the intracellular singlet oxygen levels could be successfully switched on/off through the photoconversion from OF-NPs to CF-NPs.

These above results suggested that the $^1O_2$ generation ability of supramolecular nanoparticles could be regulated by the diarylethene photoswitch in water. Therefore, we conducted experiments in living cells to investigate the controllable photodynamic therapy toward A549 cancer cells. Cell counting kit-8 (CCK-8) assay was used to determine the cytotoxicity of each sample. As expected, as shown in Figure 6d and Figure S34, both OF-NPs and CF-NPs displayed a relatively low cellular toxicity in the dark and the viability of A549 cells could still reach more than 91%. However, the viability rate of A549 cells incubated with OF-NPs decreased sharply to 12% after treatment with 30 min light irradiation, demonstrating the apparent cytotoxicity of OF-NPs under 450 nm light. In sharp contrast with OF-NPs, the viability rate of cells treated with CF-NPs could still exceed 80% under the same experimental conditions, suggesting that CF-NPs presented significantly lower phototoxicity because of the inhibition of toxic $^1O_2$ generation. Furthermore, the IC_{50} value of OF-NPs toward A549 cells was determined as low as 3.824 ± 0.201 μM under 450 nm light irradiation. These results jointly clarified the photoswitchable singlet oxygen generation behavior of the resultant supramolecular nanoparticles based on the energy transfer for controlled photodynamic therapy. Moreover, apoptosis assay was also employed to quantitatively analyze the apoptotic and necrotic cells after A549 cancer cell treatment with OF-NPs or CF-NPs under 450 nm light irradiation. As illustrated in Figure 6e and Figure S35, the cells in the control group displayed negligible apoptosis or necrosis with rates all less than 0.3%. In stark contrast, the number of apoptotic cells increased to 94.57% after treatment with OF-NPs and then exposure to light for 30 min, which was 4.68 times of that in the CF-NP group. In addition, the late apoptosis rate was significantly higher than that of early apoptosis. This result was basically consistent with cytotoxicity tests.

In addition, the photodynamic therapy effect toward 293T normal cells was also explored. 293T normal cells revealed a relatively higher viability (> 93%) in the dark or under light after incubation with CF-NPs for 24 h (Figure 6f). OF-NPs also displayed low dark toxicity with cellular viability as high as 98%. However, compared with A549 cancer cells, 293T normal cells still hold a cell viability as 82% after light irradiation, which was dramatically higher than A549 cells. In combination with the CLSM images in Figure S29 and cytotoxicity tests, these phenomena jointly suggested that OF-NPs could be selectively internalized by cancer cells benefiting from CD44-receptor-mediated endocytosis, which not only significantly prevented NPs from entering normal cells but also avoided side effects and improved the safety of photodynamic therapy. Considering the above results, this new controllable singlet oxygen generation nanosystem has exerted excellent light-responsive killing effects towards cancer cells. This not only provides a new approach for the design and construction of the water-soluble, biocompatible, responsively switchable photodynamic system but also sufficiently hints that these cyclodextrin secondary assemblies can be further developed into an anticancer nonosystem and applied into in vivo tumor therapy.

CONCLUSIONS

In summary, we have successfully constructed a cyclodextrin secondary assembly in two stages by taking advantage of the multivalent interactions among diarylethene-bridged dicyclodextrin, adamantane-polypyridyl ruthenium photosensitizers, and β-cyclodextrin-grafted hyaluronic acid. The resultant nanoparticles not only possessed favorable water solubility and biocompatibility but also possessed cancer cell-targeting ability. Crucially, the excellent photoisomerization performance of diarylethene enabled these nanoparticles to serve as a supramolecular switch for the reversible controllability of luminescence and noninvasive regulation of $^1O_2$ generation efficiency both in water and in cancer cells via alternative irradiation of UV or visible light. In vitro investigations demonstrated that these nanoparticles could specifically target A549 cancer cells rather than 293T normal cells by virtue of the CD44-mediated endocytosis. Upon light activation, the ring-open form OF-NPs displayed notable phototoxicity toward cancer cells, whereas the ring-closed form CF-NPs showed nearly negligible toxicity. Therefore, this supramolecular strategy based on responsively switchable photodynamic secondary assemblies could efficiently target cancer cells and avoid the inadvertent photosensitizer activation, which will offer a novel method for safe and high-efficiency cancer therapy.

ASSOCIATED CONTENT

Supporting Information

The Supporting Information is available free of charge at https://pubs.acs.org/doi/10.1021/acs.biomac.0c01547.

Measurements; synthesis steps of intermediate products; ^1H NMR, ^{13}C NMR, and ESI-MS spectrum of chemical compounds; emission and absorption spectrum; UV−vis absorbance changes of ABDA at different times; cellular photographs of A549 cancer cells; CLSM images of 293T normal cells; and apoptosis assay (PDF)

AUTHOR INFORMATION

Corresponding Author

Yu Liu − *Department College of Chemistry, State Key Laboratory of Elemento-Organic Chemistry, Nankai University, Tianjin 300071, China;* orcid.org/0000-0001-8723-1896; Email: yuliu@nankai.edu.cn

https://dx.doi.org/10.1021/acs.biomac.0c01547
Biomacromolecules 2020, 21, 5369−5379

Authors

Xianyin Dai − *Department College of Chemistry, State Key Laboratory of Elemento-Organic Chemistry, Nankai University, Tianjin 300071, China*

Xiaoyun Dong − *Department College of Chemistry, State Key Laboratory of Elemento-Organic Chemistry, Nankai University, Tianjin 300071, China*

Zhixue Liu − *Department College of Chemistry, State Key Laboratory of Elemento-Organic Chemistry, Nankai University, Tianjin 300071, China*

Guoxing Liu − *Department College of Chemistry, State Key Laboratory of Elemento-Organic Chemistry, Nankai University, Tianjin 300071, China;* orcid.org/0000-0003-1609-3865

Complete contact information is available at: https://pubs.acs.org/10.1021/acs.biomac.0c01547

Notes

The authors declare no competing financial interest.

■ ACKNOWLEDGMENTS

This work was financially supported by the National Natural Science Foundation of China (grant nos. 21672113, 21772099, 21861132001, 21801063, and 21971127).

■ REFERENCES

(1) Li, Z.; Li, X.; Yang, Y. W. Conjugated Macrocycle Polymer Nanoparticles with Alternating Pillarenes and Porphyrins as Struts and Cyclic Nodes. *Small* **2019**, *15*, 1805509.

(2) Chen, L.-J.; Chen, S.; Qin, Y.; Xu, L.; Yin, G.-Q.; Zhu, J.-L.; Zhu, F.-F.; Zheng, W.; Li, X.; Yang, H.-B. Construction of Porphyrin-Containing Metallacycle with Improved Stability and Activity within Mesoporous Carbon. *J. Am. Chem. Soc.* **2018**, *140*, 5049−5052.

(3) Li, W.-J.; Hu, Z.; Xu, L.; Wang, X.-Q.; Wang, W.; Yin, G.-Q.; Zhang, D.-Y.; Sun, Z.; Li, X.; Sun, H.; Yang, H.-B. Rotaxane-Branched Dendrimers with Enhanced Photosensitization. *J. Am. Chem. Soc.* **2020**, *142*, 16748−16756.

(4) Gao, Z.-Z.; Wang, Z.-K.; Wei, L.; Yin, G.; Tian, J.; Liu, C.-Z.; Wang, H.; Zhang, D.-W.; Zhang, Y.-B.; Li, X.; Liu, Y.; Li, Z.-T. Water-Soluble 3D Covalent Organic Framework that Displays an Enhanced Enrichment Effect of Photosensitizers and Catalysts for the Reduction of Protons to H_2. *ACS Appl. Mater. Interfaces* **2019**, *12*, 1404−1411.

(5) Han, J.; Liu, K.; Chang, R.; Zhao, L.; Yan, X. Photooxidase-Mimicking Nanovesicles with Superior Photocatalytic Activity and Stability Based on Amphiphilic Amino Acid and Phthalocyanine Co-Assembly. *Angew. Chem., Int. Ed.* **2019**, *58*, 2000−2004.

(6) Zhou, W.-L.; Zhao, X.; Chen, Y.; Liu, Y. Construction and heterogeneous photooxidization reactivity of a cyclodextrin/porphyrin polyrotaxane network. *Org. Chem. Front.* **2019**, *6*, 10−14.

(7) Wu, W.; Xu, S.; Qi, G.; Zhu, H.; Hu, F.; Liu, Z.; Zhang, D.; Liu, B. A Cross-linked Conjugated Polymer Photosensitizer Enables Efficient Sunlight-Induced Photooxidation. *Angew. Chem., Int. Ed.* **2019**, *58*, 3062−3066.

(8) Wu, X.; Chen, Y.; Liu, Y. Supramolecular Crosslinked Polymer for Efficient Organic Dye Removal from Aqueous Solution. *Adv. Sustainable Syst.* **2019**, *3*, 1800165.

(9) Phua, S. Z. F.; Yang, G.; Lim, W. Q.; Verma, A.; Chen, H.; Thanabalu, T.; Zhao, Y. Catalase-Integrated Hyaluronic Acid as Nanocarriers for Enhanced Photodynamic Therapy in Solid Tumor. *ACS Nano* **2019**, *13*, 4742−4751.

(10) Wu, X.; Chen, Y.; Yu, Q.; Li, F.-Q.; Liu, Y. A cucurbituril/polysaccharide/carbazole ternary supramolecular assembly for targeted cell imaging. *Chem. Commun.* **2019**, *55*, 4343−4346.

(11) Yu, G.; Yu, S.; Saha, M. L.; Zhou, J.; Cook, T. R.; Yung, B. C.; Chen, J.; Mao, Z.; Zhang, F.; Zhou, Z.; Liu, Y.; Shao, L.; Wang, S.; Gao, C.; Huang, F.; Stang, P. J.; Chen, X. A discrete organoplatinum-(II) metallacage as a multimodality theranostic platform for cancer photochemotherapy. *Nat. Commun.* **2018**, *9*, 4335.

(12) Tian, J.; Xia, L.; Wu, J.; Huang, B.; Cao, H.; Zhang, W. Linear Alternating Supramolecular Photosensitizer for Enhanced Photodynamic Therapy. *ACS Appl. Mater. Interfaces* **2020**, *12*, 32352−32359.

(13) Chen, H.; Zeng, X.; Tham, H. P.; Phua, S. Z. F.; Cheng, W.; Zeng, W.; Shi, H.; Mei, L.; Zhao, Y. NIR-Light-Activated Combination Therapy with a Precise Ratio of Photosensitizer and Prodrug Using a Host−Guest Strategy. *Angew. Chem., Int. Ed.* **2019**, *58*, 7641−7646.

(14) Irie, M. Photochromism of diarylethene single molecules and single crystals. *Photochem. Photobiol. Sci.* **2010**, *9*, 1535.

(15) Celli, J. P.; Spring, B. Q.; Rizvi, I.; Evans, C. L.; Samkoe, K. S.; Verma, S.; Pogue, B. W.; Hasan, T. Imaging and Photodynamic Therapy: Mechanisms, Monitoring, and Optimization. *Chem. Rev.* **2010**, *110*, 2795−2838.

(16) Lovell, J. F.; Liu, T. W. B.; Chen, J.; Zheng, G. Activatable Photosensitizers for Imaging and Therapy. *Chem. Rev.* **2010**, *110*, 2839−2857.

(17) Li, X.; Lee, S.; Yoon, J. Supramolecular photosensitizers rejuvenate photodynamic therapy. *Chem. Soc. Rev.* **2018**, *47*, 1174−1188.

(18) Wu, W.; Shao, X.; Zhao, J.; Wu, M. Controllable Photodynamic Therapy Implemented by Regulating Singlet Oxygen Efficiency. *Adv. Sci.* **2017**, *4*, 1700113.

(19) Shao, L.; Pan, Y.; Hua, B.; Xu, S.; Yu, G.; Wang, M.; Liu, B.; Huang, F. Constructing Adaptive Photosensitizers via Supramolecular Modification Based on Pillararene Host−Guest Interactions. *Angew. Chem., Int. Ed.* **2020**, *59*, 11779−11783.

(20) Qian, W.; Zuo, M.; Sun, G.; Chen, Y.; Han, T.; Hu, X.-Y.; Wang, R.; Wang, L. The construction of an AIE-based controllable singlet oxygen generation system directed by a supramolecular strategy. *Chem. Commun.* **2020**, *56*, 7301−7304.

(21) Roy, I.; Bobbala, S.; Young, R. M.; Beldjoudi, Y.; Nguyen, M. T.; Cetin, M. M.; Cooper, J. A.; Allen, S.; Anamimoghadam, O.; Scott, E. A.; Wasielewski, M. R.; Stoddart, J. F. A Supramolecular Approach for Modulated Photoprotection, Lysosomal Delivery, and Photodynamic Activity of a Photosensitizer. *J. Am. Chem. Soc.* **2019**, *141*, 12296−12304.

(22) Zhang, Y.-H.; Li, X.; Huang, L.; Kim, H. S.; An, J.; Lan, M.; Cao, Q.-Y.; Kim, J. S. AIE based GSH activatable photosensitizer for imaging-guided photodynamic therapy. *Chem. Commun.* **2020**, *56*, 10317−10320.

(23) Gao, J.; Li, J.; Geng, W.-C.; Chen, F.-Y.; Duan, X.; Zheng, Z.; Ding, D.; Guo, D.-S. Biomarker Displacement Activation: A General Host−Guest Strategy for Targeted Phototheranostics in Vivo. *J. Am. Chem. Soc.* **2018**, *140*, 4945−4953.

(24) Sun, H.-L.; Chen, Y.; Zhao, J.; Liu, Y. Photocontrolled Reversible Conversion of Nanotube and Nanoparticle Mediated by β-Cyclodextrin Dimers. *Angew. Chem., Int. Ed.* **2015**, *54*, 9376−9380.

(25) Cai, Y.; Guo, Z.; Chen, J.; Li, W.; Zhong, L.; Gao, Y.; Jiang, L.; Chi, L.; Tian, H.; Zhu, W.-H. Enabling Light Work in Helical Self-Assembly for Dynamic Amplification of Chirality with Photoreversibility. *J. Am. Chem. Soc.* **2016**, *138*, 2219−2224.

(26) Zhang, J.; Fu, Y.; Han, H.-H.; Zang, Y.; Li, J.; He, X.-P.; Feringa, B. L.; Tian, H. Remote light-controlled intracellular target recognition by photochromic fluorescent glycoprobes. *Nat. Commun.* **2017**, *8*, 987.

(27) Fu, Y.; Han, H.-H.; Zhang, J.; He, X.-P.; Feringa, B. L.; Tian, H. Photocontrolled Fluorescence "Double-Check" Bioimaging Enabled by a Glycoprobe−Protein Hybrid. *J. Am. Chem. Soc.* **2018**, *140*, 8671−8674.

(28) Hou, L.; Zhang, X.; Pijper, T. C.; Browne, W. R.; Feringa, B. L. Reversible Photochemical Control of Singlet Oxygen Generation Using Diarylethene Photochromic Switches. *J. Am. Chem. Soc.* **2014**, *136*, 910−913.

(29) Park, J.; Jiang, Q.; Feng, D. W.; Zhou, H. C. Controlled Generation of Singlet Oxygen in Living Cells with Tunable Ratios of

the Photochromic Switch in Metal-Organic Frameworks. *Angew. Chem., Int. Ed.* **2016**, *55*, 7188−7193.
(30) Mi, Y.; Cheng, H.-B.; Chu, H.; Zhao, J.; Yu, M.; Gu, Z.; Zhao, Y.; Li, L. A photochromic upconversion nanoarchitecture: towards activatable bioimaging and dual NIR light-programmed singlet oxygen generation. *Chem. Sci.* **2019**, *10*, 10231−10239.
(31) Zhai, Y.; Busscher, H. J.; Liu, Y.; Zhang, Z.; van Kooten, T. G.; Su, L.; Zhang, Y.; Liu, J.; Liu, J.; An, Y.; Shi, L. Photoswitchable Micelles for the Control of Singlet-Oxygen Generation in Photodynamic Therapies. *Biomacromolecules* **2018**, *19*, 2023−2033.
(32) Qin, Y.; Chen, L.-J.; Dong, F.; Jiang, S.-T.; Yin, G.-Q.; Li, X.; Tian, Y.; Yang, H.-B. Light-Controlled Generation of Singlet Oxygen within a Discrete Dual-Stage Metallacycle for Cancer Therapy. *J. Am. Chem. Soc.* **2019**, *141*, 8943−8950.
(33) Liu, G.; Xu, X.; Chen, Y.; Wu, X.; Wu, H.; Liu, Y. A highly efficient supramolecular photoswitch for singlet oxygen generation in water. *Chem. Commun.* **2016**, *52*, 7966−7969.
(34) Zhang, Y. M.; Liu, Y. H.; Liu, Y. Cyclodextrin-Based Multistimuli-Responsive Supramolecular Assemblies and Their Biological Functions. *Adv. Mater.* **2019**, *32*, 1806158.
(35) Zhang, J.; Ma, P. X. Cyclodextrin-based supramolecular systems for drug delivery: Recent progress and future perspective. *Adv. Drug Delivery Rev.* **2013**, *65*, 1215−1233.
(36) Van De Manakker, F.; Vermonden, T.; Van Nostrum, C. F.; Hennink, W. E. Cyclodextrin-Based Polymeric Materials: Synthesis, Properties, and Pharmaceutical/Biomedical Applications. *Biomacromolecules* **2009**, *10*, 3157−3175.
(37) Liu, Z.; Zhou, W.; Li, J.; Zhang, H.; Dai, X.; Liu, Y.; Liu, Y. High-efficiency dynamic sensing of biothiols in cancer cells with a fluorescent β-cyclodextrin supramolecular assembly. *Chem. Sci.* **2020**, *11*, 4791−4800.
(38) Pei, Q.; Hu, X.; Wang, L.; Liu, S.; Jing, X.; Xie, Z. Cyclodextrin/Paclitaxel Dimer Assembling Vesicles: Reversible Morphology Transition and Cargo Delivery. *ACS Appl. Mater. Interfaces* **2017**, *9*, 26740−26748.
(39) Yu, G.; Zhao, X.; Zhou, J.; Mao, Z.; Huang, X.; Wang, Z.; Hua, B.; Liu, Y.; Zhang, F.; He, Z.; Jacobson, O.; Gao, C.; Wang, W.; Yu, C.; Zhu, X.; Huang, F.; Chen, X. Supramolecular Polymer-Based Nanomedicine: High Therapeutic Performance and Negligible Long-Term Immunotoxicity. *J. Am. Chem. Soc.* **2018**, *140*, 8005−8019.
(40) Nalluri, S. K. M.; Voskuhl, J.; Bultema, J. B.; Boekema, E. J.; Ravoo, B. J. Light-Responsive Capture and Release of DNA in a Ternary Supramolecular Complex. *Angew. Chem., Int. Ed.* **2011**, *50*, 9747−9751.
(41) Ooi, Y. J.; Wen, Y.; Zhu, J.; Song, X.; Li, J. Surface Charge Switchable Polymer/DNA Nanoparticles Responsive to Tumor Extracellular pH for Tumor-Triggered Enhanced Gene Delivery. *Biomacromolecules* **2020**, *21*, 1136−1148.
(42) Yu, Q.; Zhang, B.; Zhang, Y.-M.; Liu, Y.-H.; Liu, Y. Actin Cytoskeleton-Disrupting and Magnetic Field-Responsive Multivalent Supramolecular Assemblies for Efficient Cancer Therapy. *ACS Appl. Mater. Interfaces* **2020**, *12*, 13709−13717.
(43) Sun, C.; Wang, Z.; Yue, L.; Huang, Q.; Cheng, Q.; Wang, R. Supramolecular Induction of Mitochondrial Aggregation and Fusion. *J. Am. Chem. Soc.* **2020**, *142*, 16523−16527.
(44) Zhang, Y.-M.; Zhang, N.-Y.; Xiao, K.; Yu, Q.; Liu, Y. Photo-Controlled Reversible Microtubule Assembly Mediated by Paclitaxel-Modified Cyclodextrin. *Angew. Chem., Int. Ed.* **2018**, *57*, 8649−8653.
(45) Zhou, W.-L.; Chen, Y.; Yu, Q.; Zhang, H.; Liu, Z.-X.; Dai, X.-Y.; Li, J.-J.; Liu, Y. Ultralong purely organic aqueous phosphorescence supramolecular polymer for targeted tumor cell imaging. *Nat. Commun.* **2020**, *11*, 4655.
(46) Nam, J. S.; Kang, M.-G.; Kang, J.; Park, S.-Y.; Lee, S. J. C.; Kim, H.-T.; Seo, J. K.; Kwon, O.-H.; Lim, M. H.; Rhee, H.-W.; Kwon, T.-H. Endoplasmic Reticulum-Localized Iridium(III) Complexes as Efficient Photodynamic Therapy Agents via Protein Modifications. *J. Am. Chem. Soc.* **2016**, *138*, 10968−10977.
(47) Jeena, M. T.; Palanikumar, L.; Go, E. M.; Kim, I.; Kang, M. G.; Lee, S.; Park, S.; Choi, H.; Kim, C.; Jin, S.-M.; Bae, S. C.; Rhee, H. W.; Lee, E.; Kwak, S. K.; Ryu, J.-H. Mitochondria localization induced self-assembly of peptide amphiphiles for cellular dysfunction. *Nat. Commun.* **2017**, *8*, 26.

https://dx.doi.org/10.1021/acs.biomac.0c01547
Biomacromolecules 2020, 21, 5369−5379